Chapter 8
Beam–Beam Effects

V. Shiltsev and A. Valishev

8.1 Beam–Beam Effects in Tevatron: Introduction

Beam–beam effects became a subject of study as soon as there were colliders beginning with the first *e*+*e*− collider AdA in Frascati that started operating in 1962 and the first *p*–*p* collider ISR at CERN that started operating in 1971. Over the years many different issues related to electromagnetic interactions of colliding beams have emerged. In the Tevatron collider, the beam–beam problems take place in the context of beam losses and emittance growth due to long-range and head-on interactions. A comparative review of beam–beam performance of a number of hadron colliders [1] shows that the beam parameters operationally achieved in the Tevatron correspond to record high incoherent tune shift due to collisions (the figure of merit of beam–beam interaction):

$$\xi = N_{\mathrm{IP}} \frac{N_{\mathrm{p}} r_{\mathrm{p}}}{4\pi\varepsilon} \approx 0.025 - 0.030, \tag{8.1}$$

where r_{p} denotes the classical proton radius, N_{p} and ε are the opposite bunch intensity and emittance, correspondingly. Remarkably, the Tevatron working points (vertical and horizontal tunes) lie above the half integer between the fifth- and seventh-order resonances (between 3/5 = 0.6 and 4/7 = 0.571) and the beam–beam tune spread fully covers the tune area.

During the Collider Run II, beam losses during injection, ramp and squeeze phases were mostly caused by beam–beam effects. Figure 8.1 from [2] shows that

V. Shiltsev (✉) • A. Valishev
Fermi National Accelerator Laboratory, Accelerator Physics Center, PO Box 500, MS 221, Batavia, IL 60510, USA
e-mail: shiltsev@fnal.gov

V. Lebedev and V. Shiltsev (eds.), *Accelerator Physics at the Tevatron Collider*, Particle Acceleration and Detection, DOI 10.1007/978-1-4939-0885-1_8,

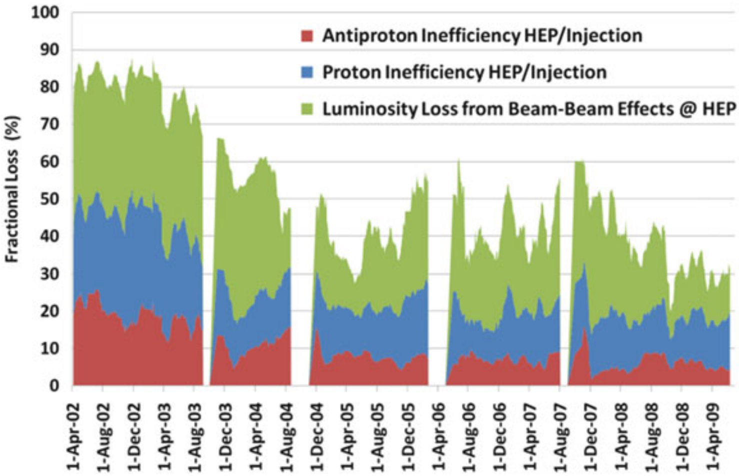

Fig. 8.1 Evolution of beam losses in 2002–2009. *Red* shows fractional loss of antiprotons between injection into the Tevatron and start of collisions, next (*blue*) one is for loss of protons, *green*—fractional reduction of the luminosity integral caused by beam–beam effects in collisions [2]

early in Run II, combined beam losses only in the Tevatron (the last accelerator out of total 7 in the accelerator chain) claimed significantly more than half of the integrated luminosity. Due to various improvements, losses have been reduced significantly down to some 20–30 % in 2008–2009, paving the road to a many-fold increase of the luminosity. In "proton-only" or "antiproton-only" stores, the losses do not exceed 2–3 %. So, the remaining 8–10 % proton loss and 2–3 % antiproton loss are caused by beam–beam effects, as well as some 5–10 % reduction of the luminosity lifetime in collision. Note that the proton inefficiency is higher than the antiproton one, despite the factor of 3–5 higher proton intensity. That is explained in the following chapters by significantly smaller antiproton emittances.

Beam–beam interactions differ between the injection and collision stages. The helical orbits should provide sufficient separation between the proton and antiproton beams in order to reduce detrimental beam–beam effects, e.g., tune shifts, coupling, and high-order resonance driving terms. Each bunch experiences 72 long-range interactions per revolution at injection, but at collision there are 70 long-range interactions and two head-on collisions per bunch at the CDF and D0 detectors—see Fig. 8.2. In total, there are 138 locations around the ring where beam–beam interactions occur. The sequence of 72 interactions out of the 138 possible ones differs for each bunch; hence the effects vary from bunch to bunch. The locations of these interactions and the beam separations change from injection to collision because of the antiproton cogging (relative timing between antiprotons and protons).

Initially, there were six separator groups (three horizontal and three vertical) in the arcs between the two main interaction points, *B*0 (CDF) and *D*0. During collisions, these separators form closed orbit 3-bumps in each plane. However,

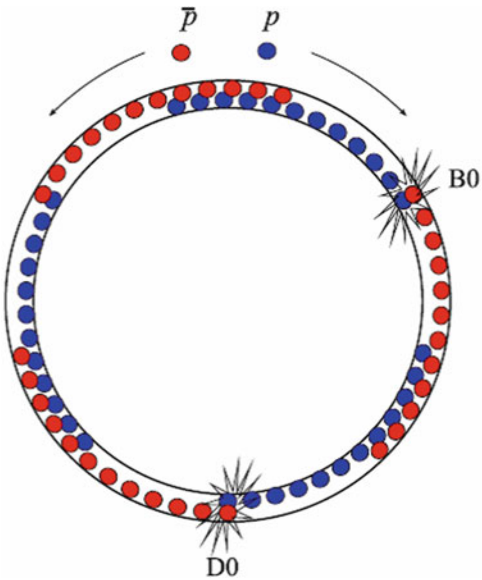

Fig. 8.2 Schematic of proton (*blue*) and antiproton (*red*) bunches in the Tevatron and the two head-on collision locations $B0$ and $D0$

the condition of orbit closure prevented running the separators at maximum voltages with exception for horizontal separators in the short arc from $B0$ to $D0$. This limited separation at the nearest parasitic crossings 59 m away from the main IPs aggravating the long-range beam–beam interaction. To increase separation at these parasitic crossings three additional separators were installed as to create closed orbit 4-bumps both in horizontal and vertical planes in the long arc (from $D0$ to $B0$) and in the vertical plane in the short arc.

There is more flexibility in the helix design for the preceding stages: injection, ramp, and squeeze. There are still some difficulties at these stages, including:

1. Irregularities in betatron phase advance over the straight sections, especially $A0$.
2. Aperture restrictions (physical as well as dynamic) that limit the helix amplitude at injection and at the beginning of the ramp.
3. The maximum separator voltage gradient of 48 kV/cm (limited by separator spark rate) leads to a faster drop in separation, $d \sim 1/E$, than in the beam size, $\sigma \sim 1/E^{1/2}$, during the second part of the ramp above the energy of $E = 500$ GeV.
4. The polarity reversal of the horizontal separation during the squeeze (to satisfy needs of HEP experiments) that leads to a short partial collapse of the helix.

A simple figure of merit is helpful when comparing different helix designs. The conventional choice is the *minimum* value of the so-called *radial separation*, S, over all possible parasitic interaction crossing points in units of the RMS betatron beam sizes $\sigma_{x,y\beta}$:

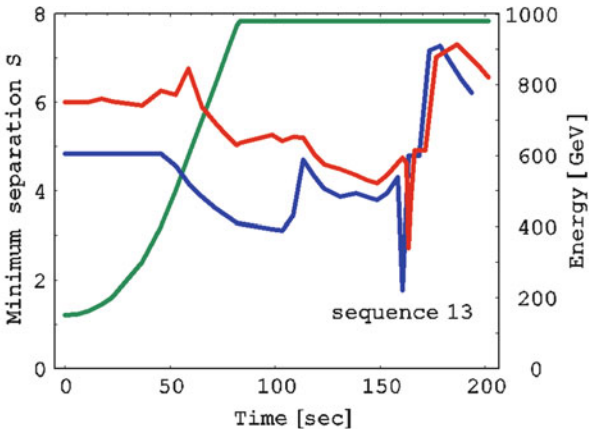

Fig. 8.3 Minimum radial separation, Eq. (8.2), on ramp and during the low-beta squeeze. The *green line* represents the beam energy on the ramp $E(t)$. The *blue* and *red lines* represent $S(t)$ for the helix configurations used ca. January 2002 and August 2004, respectively [7]

$$S = \sqrt{\left(\Delta x/\sigma_{x\beta}\right)^2 + \left(\Delta y/\sigma_{y\beta}\right)^2}. \tag{8.2}$$

The separation is normalized to a fixed reference emittance of 2.5 π mm mrad. Our experience has shown that less than 5–6σ separation causes unsatisfactory losses. Figure 8.3 shows the minimum radial separation S during the ramp and squeeze with the initial helix design (blue, ca. January 2002) and an improved helix (red, ca. August 2004). The long-range interactions contribute a tune spread of about [3]:

$$\Delta Q \approx \sum_{\text{parasitic encounters}} \frac{2\xi}{S^2} \approx 0.008, \tag{8.3}$$

as well as several units of chromaticity [4]. In the end of Run II operations, both species had about the same beam–beam tune shifts and are effectively in the strong–strong regime. That is because of much smaller antiproton emittances which were available due to electron cooling of antiprotons in the Recycler, starting in 2005. Consequently the antiprotons effectively experience only the linear part of the head-on beam–beam force and do not suffer much from it. Since 2006, antiproton losses due to beam–beam interactions during stores have been small, provided the tunes are well controlled. Protons on the other hand have tunes closer to twelfth-order resonances and are transversely larger than the antiprotons. Consequently during head-on collisions, they experience the nonlinear beam–beam force enhanced by chromatic effects and suffer beam loss and emittance growth. A review of beam–beam observations in Run I can be found in [5, 6].

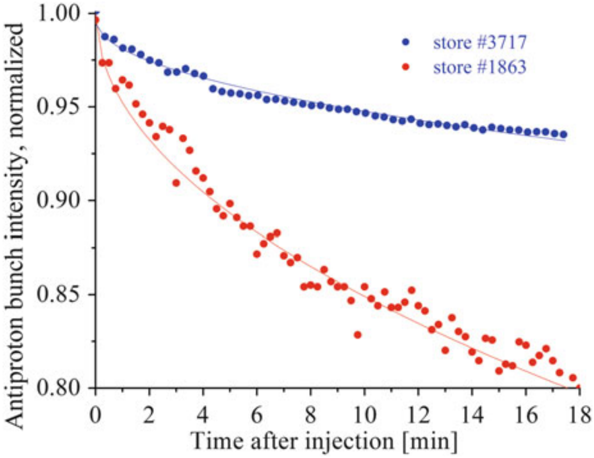

Fig. 8.4 Decay of (normalized) intensity for antiproton bunch #1 at injection. The *red dots* are for store #1863 (October 16, 2002) and the *blue dots* are store #3717 (August 8, 2004). The *blue* and *red lines* represent fits according to $N(t) = N_0 e^{-\sqrt{t/\tau}}$ with parameters $N_0 = 32.5 \times 10^9$, $\tau = 7.4$ h and $N_0 = 55.7 \times 10^9$, $\tau = 69.8$ h, respectively [7]

8.2 Beam–Beam Phenomena in Tevatron Operation

8.2.1 Long-Range Beam–Beam Interaction Effects at Injection, on the Energy Ramp and During Low-Beta-Squeeze

Before being brought to collisions, the Tevatron beams are transversely separated during the entire injection process, during energy ramp from 150 to 980 GeV and low-beta squeeze. Long-range beam–beam interaction leads to particle losses at these stages. In the absence of opposite beam, the combined losses are small, of the order of ~2–4 %, as measured during dedicated proton-only and antiproton-only stores.

Although both the proton and antiproton beams stay at 150 GeV for less than an hour, a significant particle loss occurred during that time at the beginning of the Run II. The particle losses for both beams were driven by diffusion and exacerbated by small transverse and longitudinal apertures. Figure 8.4 presents the intensity lifetimes of single antiproton bunches after injection for typical stores in 2002 and 2004. It is clearly seen for both stores that the intensity decay is not exponential. Figure 8.4 shows that the intensities are approximated well by the expression $N(t) = N_0 e^{-\sqrt{t/\tau}}$ that was used for the lifetime fits. Similar $\sqrt{t}$ dependence has been observed for the bunch length "shaving" (slow reduction of the rms bunch length), while transverse emittances do not exhibit such dependence on $\sqrt{t}$ and usually either stay flat or slightly grow [7].

During approximately 20 min needed to load antiprotons into the Tevatron, the proton lifetime degrades as more antiproton bunches are injected. Figure 8.5 shows an approximately linear dependence of the proton loss rate at 150 GeV on the number of antiprotons in the Tevatron. The proton loss rate without antiprotons is about 4 % per hour (25 h lifetime), whereas it grows to about 16 % per hour (6 h

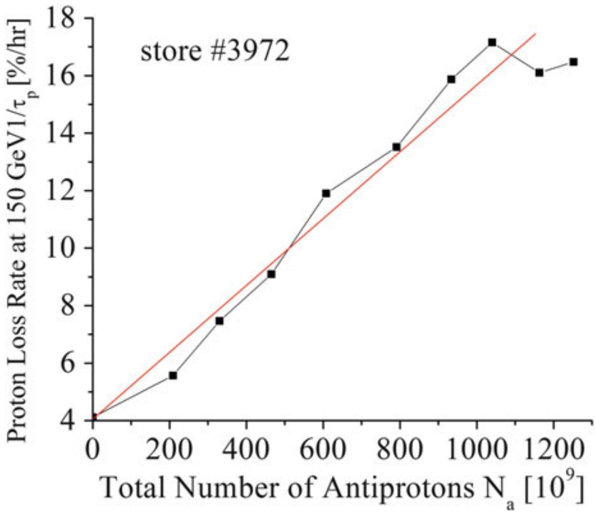

Fig. 8.5 Proton intensity loss rate at the 150 GeV helix in units of %/h vs. total number of antiprotons injected into the Tevatron N_a during shot setup #3972 (February 8, 2005). The points are the results of ordinary exponential decay fits over 2 min after each antiproton injection. The *solid red line* is the linear fit $1/\tau_p[\%/h] = 4 + 11.6(N_a/1{,}000)$ (from [1])

lifetime) when all antiproton bunches are loaded. A similar linear dependence of the antiproton loss rate on proton intensity can be seen as well.

Besides being dependent on the intensity of the opposing beam, the particle losses due to the long-range beam–beam interaction at injection, ramp, and squeeze are found to be dependent on beam emittances and chromaticities, approximately as [7, 8]

$$\frac{\Delta N_{\mathrm{a,p}}}{N_{\mathrm{a,p}}} = 1 - \frac{N(t)}{N(t=0)} \propto \sqrt{t} \cdot \varepsilon^2_{\mathrm{a,p}} \frac{N_{\mathrm{p,a}}}{\varepsilon_{\mathrm{p,a}}} Q'^2{}_{\mathrm{a,p}} \cdot F\left(\varepsilon_{\mathrm{L}}, Q_{x,y}, S_{\mathrm{a-p}}\right), \tag{8.4}$$

where the index a or p stands for antiprotons or protons, ε is transverse emittance, N is total number of particles in the opposite beam, Q' is the chromaticity on the corresponding helix, and the factor F emphasizes the fact that losses also depend on the longitudinal emittance ε_L, separation S (size of the helix and cogging stage), and tune Q. Over years of operation, the betatron tunes on both helices at injection and ramp were optimized to be close to $Q_x/Q_y = 20.584/20.576$, i.e., above seventh-order resonances at 4/7=0.5714, but close to the twelfth-order resonance 7/12=0.5833. Significant variations of the tune (in excess of ±0.002) often led to lifetime reduction, especially if the vertical tune approached the 4/7 resonance.

Equation (8.4) above emphasizes the importance of chromaticity for reducing the losses of both protons and antiprotons. Since the proton and antiproton orbits are separated using the electrostatic separators, their tunes and chromaticities can be controlled independently by using sextupole and octupole circuits, respectively. The major obstacle in attaining the desired chromaticity reduction was a weak head-tail instability in high intensity proton bunches [9]. Early in Run II, avoiding this instability required chromaticities as high as 8–12 units at 150 GeV. Reducing the proton chromaticities down to +(3–4) units became possible after removing unused high-impedance extraction Lambertson magnets, reducing the impedance of the injection Lambertson magnets by installing conductive liners, and commissioning active bunch-by-bunch instability dampers for the protons [10]. Decreasing the chromaticities to zero has become possible after reconfiguring octupole circuits to introduce Landau damping to suppress the head-tail instability. The antiproton bunches do not suffer from that instability since the intensity is much smaller than that of protons. Consequently, both Q'_x and Q'_y are set closer to 0 by using differential chromaticity octupole circuits.

The observed $\sqrt{t}$ dependence of beam intensity decay (see Fig. 8.4) and bunch length is believed to be due to particle diffusion that leads to particle loss at physical or dynamic apertures. The major diffusion mechanisms are intrabeam scattering (IBS), scattering on the residual gas, and diffusion caused by RF phase noise. For example, if the available machine aperture is smaller than the beam size of the injected beam, the beam is clipped on the first turn with an instantaneous particle loss. Such a clipping creates a step-like discontinuity at the boundary of the beam distribution that causes very fast particle loss due to diffusion. The diffusion wave propagates inward, so that the effective distance is proportional to $\sqrt{t}$. Consequently, the particle loss is also proportional to $\sqrt{t}$. To estimate such a "worst-case loss," consider an initially uniform beam distribution: $f(I) = f_0 \equiv 1/I_0$, where I_0 is the action at the boundary. For sufficiently small time, $t \ll I_0/D$, where D is diffusion coefficient, the diffusion can be considered one-dimensional in the vicinity of the beam boundary. Solving the diffusion equation

$$\frac{\partial f}{\partial t} = D \frac{\partial}{\partial I}\left(I \frac{\partial f}{\partial I}\right) \tag{8.5}$$

gives the result:

$$f(I,t) = \frac{2f_0}{\sqrt{\pi}} \int_0^{(I_0 - I)/\sqrt{4I_0 Dt}} e^{-\xi^2} d\xi. \tag{8.6}$$

By integrating it over I, one obtains the dependence of particle population on time:

$$\frac{N(t)}{N_0} \approx 1 - \sqrt{\frac{t}{\tau}}, \quad \tau = \frac{\pi I_0}{4D}, \quad t \ll \tau. \tag{8.7}$$

In the transverse degree of freedom, the Tevatron acceptance at 150 GeV on the helical orbit is about ${I^{\mathrm{tr}}}_0 \approx 8$–$13\pi$ mm mrad, depending on the pre-shot machine tune-up, while the emittance growth rate is about $D^{\mathrm{tr}} \approx 0.15$–$0.25\pi$ mm mrad/h chiefly from scattering on residual gas. So from (8.7), one can obtain a lifetime of $\tau \approx 30$–80 h. In addition, diffusion in the longitudinal plane with a rate $D^{\mathrm{long}} \approx 0.03$–$0.3$ rad^2/h can lead to lifetimes of $\tau \approx 10$–100 h in the case where the longitudinal aperture is limited only by the RF bucket size $\sqrt{{I_0}^{\mathrm{long}}} \approx 2$ rad. The above numbers are not well known, but we believe they are in the indicated ranges.

In reality, the machine acceptance is set by the interplay between the physical and dynamic apertures. The latter is a strong function of the synchrotron action, and beam–beam interactions drastically reduce the dynamic aperture for synchrotron oscillation amplitudes close to the bucket size. Naturally, such an aperture reduction is stronger for larger values of chromaticity.

The problem was alleviated significantly by a comprehensive realignment of many Tevatron elements in 2003–2004, as well as a reduction in the longitudinal emittances due to improvements in the Main Injector's bunch coalescing, and an increase of the Tevatron's dynamic aperture.

8.2.2 Beam–Beam Interaction Effects During Colliding HEP Stores

After the beams are brought into collisions at the main IPs, there are two head-on and 70 long-range collision points per bunch. Correspondingly, the beam–beam phenomena in the Tevatron collider are characterized by a complex mixture of long-range and head-on interaction effects, record high beam–beam parameters for both protons and antiprotons (the head-on tune shifts up to about $\xi = 0.03$ for both protons and antiprotons, in addition to long-range tune shifts of $\Delta Q^{\mathrm{p}} = 0.003$ and $\Delta Q^{\mathrm{a}} = 0.006$, respectively), and remarkable differences in beam dynamics of individual bunches. All that may result in the significant emittance growth and particle losses in both beams. During the running prior to the 2006 shutdown the beam–beam effects at HEP mostly affected antiprotons. The long-range collision points nearest to the main IPs were determined to be the leading cause for poor lifetime. Additional electrostatic separators were installed in order to increase the separation at these IPs from 5.4 to 6 [10]. Also, the betatron tune chromaticity was decreased from 20 to 10 units. Since then, the antiproton lifetime was dominated by losses due to luminosity and no emittance growth is observed provided that the betatron tune working point is well controlled. Electron cooling of antiprotons in the Recycler and increased antiproton intensities and brightness drastically changed the situation for protons. Figure 8.6 shows the evolution of total head-on beam–beam tune shift $\xi_{\mathrm{p.a}}$ for protons and antiprotons. Note that prior to the 2006 shutdown the proton ξ_{p} was well under 0.01 and a big boost occurred in 2007 when both beam–beam parameters became essentially equal. It was then when beam–beam-related losses and emittance blowup started to be observed in protons.

The analysis [11] showed that deterioration of the proton lifetime was caused by a decrease of the dynamical aperture for off-momentum particles due to head-on collisions. It was discovered that the Tevatron optics had large chromatic perturbations, e.g., the value of β^* for off-momentum particles could differ from that of the reference particle by as much as 20 %. Also, the high value of second-order betatron tune chromaticity $Q'' = d^2Q/d(\Delta p/p)^2$ generated a tune spread of about 0.002. A rearrangement of sextupole magnet circuits in order to correct the

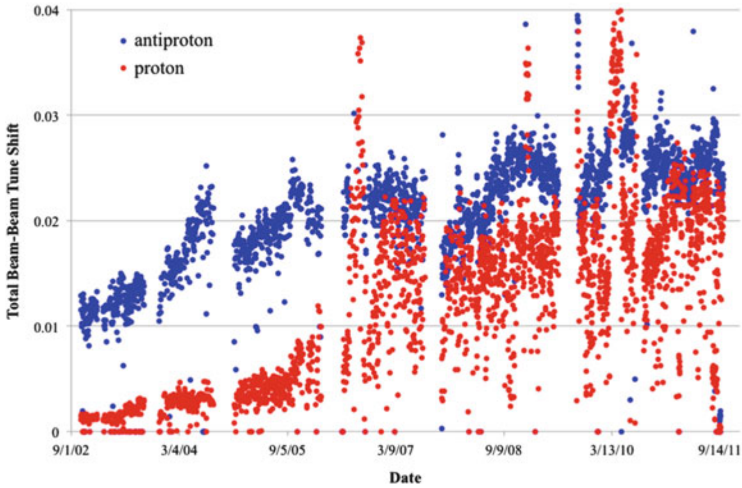

Fig. 8.6 Head-on beam–beam tune shift parameters for protons and antiprotons vs. time [8]

second-order chromaticity was planned and implemented before the 2007 shutdown [11] and led to some 10 % increase in the luminosity integral per store.

Another step up in the proton ξ_p happened after the 2007 shutdown when the transverse antiproton emittance decreased because of improvements in injection matching. The total attained head-on beam–beam tune shift for protons exceeded that of antiprotons and reached 0.028. This led to high sensitivity of the proton lifetime to small variations of the betatron tunes, and to severe background conditions for the experiments. The reason is believed to be the large betatron tune spread generated by collisions of largely different size bunches [12]. Indeed, at times the antiproton emittance was a factor of 5–6 smaller than the proton emittance. To decrease the proton to antiproton emittance ratio a system has been commissioned which increases the antiproton emittance after the top energy is reached by applying wide band noise to a directional strip line [13]. At the end of Run II, the optimal emittance ration was kept at $\varepsilon_p/\varepsilon_a \approx 3$. Below we summarize major beam–beam phenomena during HEP stores.

The beam–beam effects in the Tevatron cause nearly every measurable indicator of beam dynamics to vary as a function of position within a bunch train. As mentioned, the 36 bunches for each beam are arranged in three trains of 12 bunches each, and the variation of intensities and emittances among the proton bunches is small. Consequently, a threefold symmetry is expected [14] in the antiproton bunch dynamics. We have observed such behavior in essentially every indicator. For example, Fig. 8.7 shows that the helical orbits of antiproton bunches at the low-beta stage differ by some 40–50 μm in a systematic, ladder-like fashion (due to symmetry, the plot refers only to a single train of 12 bunches). Such variation in the closed orbits was predicted before the start of the Collider Run II [15] and

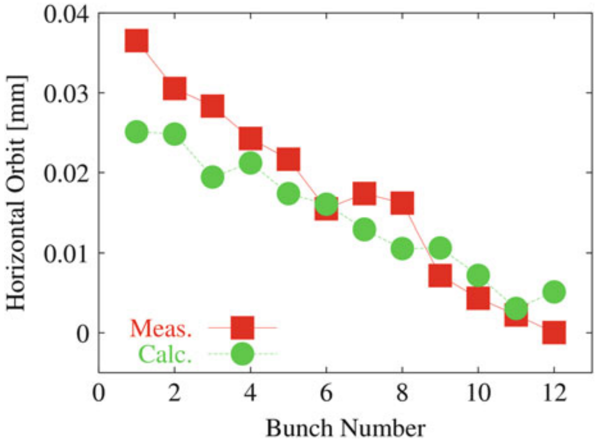

Fig. 8.7 Antiproton orbit variations along the bunch train: horizontal positions measured by synchrotron radiation monitor in collisions in store #3530 (May 23, 2004) (*red squares*) and calculated (*green circles*); for comparison, RMS horizontal betatron size of 2.5π mm mrad normalized emittance beam at the location of the monitor is equal to 0.3 mm [7]

agrees well with analytical calculations (see the comparisons in Fig. 8.7 and discussion in the next section). Vertical variation is similar and of the same order, proton orbits exhibit proportionally (to intensity) smaller bunch-by-bunch variations.

Two (vertical and horizontal) 1.7 GHz Schottky detectors [16] allow continuous, nondestructive measurements of betatron tunes and chromaticities for each proton and antiproton bunch during HEP stores. The tunes measured by the detectors represent an average over all particles in a bunch. The tune and chromaticity accuracies for single bunch measurements are better than 0.001 and 1 unit, respectively. A single measurement can be made in approximately 20 s.

Figure 8.8 presents the distribution of antiproton vertical and horizontal tunes and chromaticities along antiproton bunch train. It is remarkable that bunches #1 and #12 have vertical and horizontal tunes, respectively, much lower (by more than 0.003) than the other ten bunches. Long-range beam–beam interactions at the parasitic IPs produce such significant bunch-by-bunch tune differences ΔQ_{LR}. The data shown in Fig. 8.8 agree with analytic calculations [17, 18] if one takes into account that the measured tune is averaged over a weighted particle distribution, and, thus, the effective head-on tune shift is approximately half of the maximum beam–beam incoherent tune shift:

$$\Delta Q \approx \Delta Q_{\mathrm{LR}} + 0.5 \cdot \xi, \quad \xi = \frac{r_{\mathrm{p}} N_{\mathrm{p}}}{4\pi\varepsilon_{\mathrm{p}}} \times 2. \tag{8.8}$$

For nominal bunch parameters at the beginning of an HEP stores, the head-on tune shift is about $\xi \approx 0.020$ for antiprotons. Figure 8.9 displays the Tevatron beam tunes at the beginning of a high-luminosity HEP store on a resonance plot. Particles with up to 6σ amplitudes are presented. Small amplitude particles have tunes near the tips of the "ties" depicted for all 36 proton and 36 antiproton bunches. The most detrimental effects occur when particle tunes approach the resonances. For

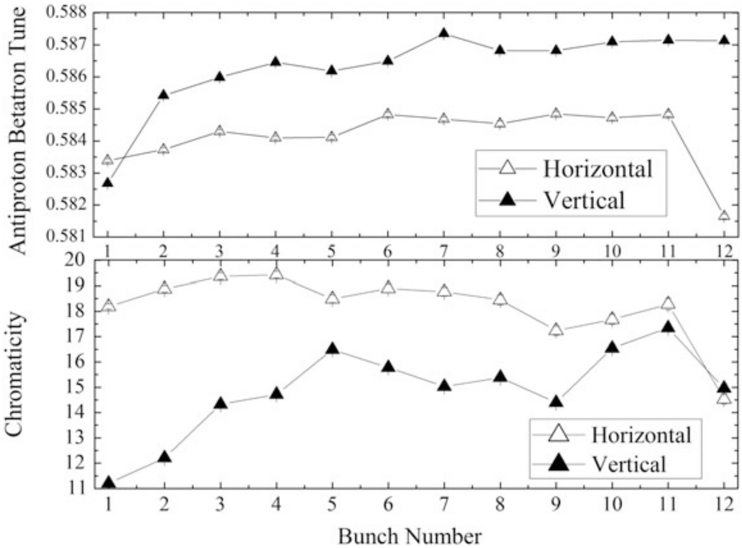

Fig. 8.8 Antiproton tunes (*top*) and chromaticities (*bottom*) measured by the 1.7 GHz Schottky monitor vs. bunch number for store #3678 (July 27–28, 2004). The tune data were taken over a period of 3 h, starting 3 h after the beginning of the store and extrapolated linearly to the time $t = 3$ h into the store. The chromaticities were assumed to be constant, and so the measurements were averaged over the entire store. The symbol size reflects the size of the statistical error bars [7]

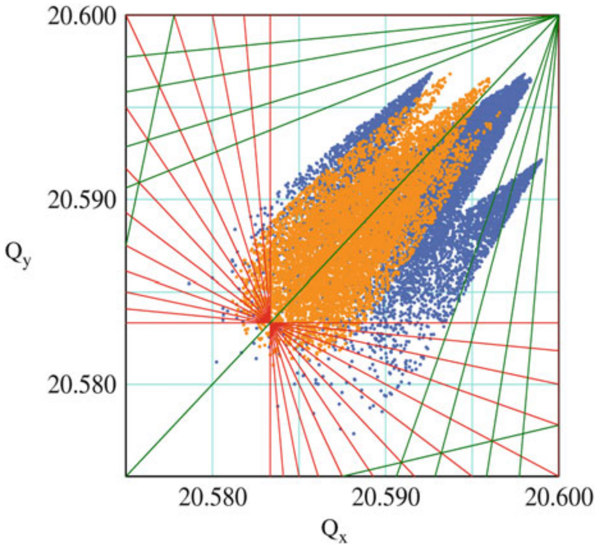

Fig. 8.9 Tevatron proton and antiproton tune distributions superimposed onto a resonance line plot. The *red* and *green lines* are various sum and difference tune resonances of up to twelfth order. The *blue dots* represent calculated the tune distributions for all 36 antiproton bunches; the *yellow* represent the protons. The tune spread for each bunch is calculated for particles up to 6σ amplitude taking into account the *measured* intensities and emittances (from [19])

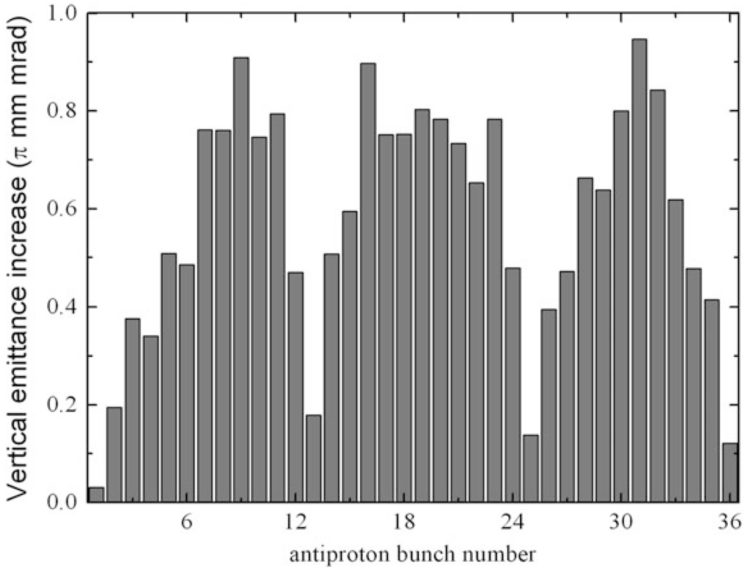

Fig. 8.10 Antiproton bunch emittance increase over the first 10 min after initiating collisions for HEP store #3231 with an initial luminosity $L = 48 \times 10^{30}\text{cm}^{-2}\ \text{s}^{-1}$ [19]

example, an emittance growth of the core of the beam is observed near the fifth-order resonances (defined as $nQ_x + mQ_y = 5$, such as $Q_{x,y} = 3/5 = 0.6$) or fast halo particle loss near twelfth-order resonances (for example, $Q_{x,y} = 7/12 \approx 0.583$).

The measured antiproton tunes decrease over the course of a store by some 0.005–0.007 with characteristic decay times of 12–16 h, caused by the reduction of the head-on tune shift, which itself is mostly due to the increase of proton emittances (by more than factor of 2) and the decrease of proton bunch intensities (by more than 25 %). Such excursions were found detrimental for luminosity lifetime were minimized by manual tuning as soon as 1.7 GHz Schottky monitors were made operational in 2005, resulting in increased beam lifetime. The chromaticities measured by the 1.7 GHz Schottky monitor are remarkably stable within 1 unit during the store and vary by about 6 units in both planes along a bunch train, and that is in acceptable agreement with theory.

It is not surprising that with such significant differences in orbits, tunes, and chromaticities, the antiproton bunch intensity lifetime and emittance growth rates vary considerably from bunch to bunch. As an illustration, Fig. 8.10 shows the vertical emittance blowup early in an HEP store for all three trains of antiproton bunches. One can see a remarkable distribution along the bunch train which gave rise to the term “scallops” (three “scallops” in three trains of 12 bunches) for this phenomenon—the end bunches of each train exhibit lower emittance growth than the bunches in the middle of the train. Because of the threefold symmetry of the proton loading, the antiproton emittance growth rates are the same within 5–20 % for corresponding bunches in different trains (in other words, bunches #1, #13, and

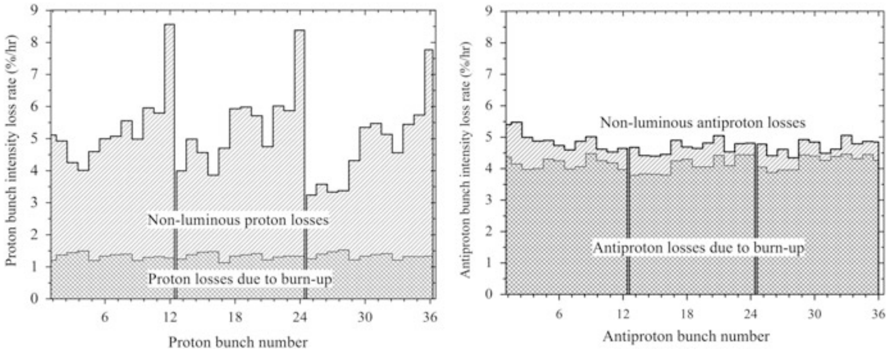

Fig. 8.11 (**a**) *Left*—proton-bunch intensity loss rates and (**b**) *right*—antiproton bunch intensity loss rates at the beginning of the Tevatron store #5155, Dec. 30, 2006, with an initial luminosity $L = 250 \times 10^{30}\ \mathrm{cm}^{-2}\ \mathrm{s}^{-1}$ (from [19])

#25 have similar emittance growths). The effect is dependent on the antiproton tunes, particularly on how close each bunch is to some important resonances—in case of the Tevatron working point, these are fifth-order (0.600), seventh-order (0.5714), and twelfth-order (0.583) resonances. For example, "the scallops" occur near the fifth-order resonances $nQ_x+mQ_y = 5$, such as $Q_{x,y} = 3/5=0.6$. Smaller but still definite "scallops" were also seen in protons if the proton tunes are not optimally set. After the initial 0.5–1 h of each store, the growth rate of each bunch decreased significantly. Various methods have been employed to minimize the development of scallops (including a successful attempt to compensate one bunch emittance growth with a Tevatron Electron Lens—see [19] and next section), but carefully optimizing the machine tunes was found to be the most effective—e.g., the vertical tune changes as small as −0.002 resulted in significant reduction of the amplitude of the "scallops."

As mentioned above, significant attrition rate of protons and antiprotons due to their interaction with opposite beam, both in the main IPs and in the numerous long-range interaction regions is one of the most detrimental effects of the beam–beam interaction in the Tevatron. The effect varies bunch-by-bunch and it is especially large at the beginning of the HEP stores where the total proton beam–beam tune shift parameter is peaked. Figure 8.11a shows a typical distribution of proton loss rates $(dN_p/N_p)/dt$ at the beginning of a high-luminosity HEP store. Bunches #12, 24, and 36 at the end of each bunch train typically lose about 9 % of their intensity per hour while other bunches lose only 4–6 % per hour. These losses are a very significant part of the total luminosity decay rate of about 20 % per hour (again, at the beginning of the high-luminosity HEP stores). The losses due to luminosity "burn-up" — inelastic proton–antiproton interactions $dN_p/dt = -\sigma_{\mathrm{int}} \cdot L$ at the two main IPs ($\sigma_{\mathrm{int}} = 0.07$ barn) are small (1–1.5 %/h) compared to the total losses. Losses due to inelastic interaction with the residual vacuum and due to leakage from the RF buckets are less than 0.3 %/h. The single largest source of proton losses is the beam–beam interaction with the antiprotons. Such conclusion is also supported by Fig. 8.11a, which shows a large bunch-to-bunch variation in the proton loss rates within each bunch train, but very similar rates for equivalent bunches, e.g., bunches #12, 24, and 36. On the contrary, antiproton intensity losses dN_a/dt are about the same for all the bunches—see Fig. 8.11b—as they are mostly due to luminosity burn-up and not determined by beam–beam effects (the latter indicated as “non-luminous” component of the loss rate).

The remarkable distribution of the proton losses seen in Fig. 8.11, e.g., particularly high loss rates for bunches #12, 24, 36, is usually thought to be linked to the distribution of betatron frequencies along the bunch trains bunch. Bunches at the end of the trains have their vertical tunes closer to the $7/12 \approx 0.583$ resonance lines, and, therefore, the higher losses. The average Tevatron proton tune Q_y of about 0.588–0.589 lies just above this resonance, and the bunches at the end of each train, whose vertical tunes are lower by $\Delta Q_y = -(0.002–0.003)$ due to the unique pattern of long-range interactions, are subject to stronger beam–beam effects. The tunes Q_y and Q_x are carefully optimized by the operation crew to minimize the overall losses of intensity and luminosity. For example, an increase of the average vertical tune by quadrupole correctors is not possible because it usually results in higher losses and “scallops” as small amplitude particle tunes move dangerously close to the $3/5 = 0.600$ resonance. The Tevatron Electron Lenses did reduce by a factor of >2 the proton losses out of the bunches #12, 24, 36 (see [19, 20] and next section).

The proton loss rate was also strongly affected by transverse size mismatch for head-on collisions of larger size proton bunches with smaller size antiproton bunches. Our studies of this phenomenon in 2003–2005 can be summarized by the following scaling formulae [7]:

$$\frac{1}{\tau_{\rm p}} = \frac{1}{N_{\rm p}}\frac{dN_{\rm p}}{dt} \propto N_{\rm a} \cdot \left(\frac{\varepsilon_{\rm p}}{\varepsilon_{\rm a}}\right)^2 F_2\left(Q_{x,y}, Q', Q'', M\right), \tag{8.9}$$

where M stands for bunch position in bunch train. In order to avoid large emittance ratio $\varepsilon_{\rm p}/\varepsilon_{\rm a}$, the antiproton emittances are routinely diffused at the beginning of HEP stores by a wide band transverse noise to a directional strip line, so the ratio is kept about 3. Factor F_2 in Eq. (8.9) shows significant dependence of the losses on the second-order betatron tune chromaticity $Q''=d^2Q/d(\Delta p/p)^2$. As mentioned at the beginning of this section, the second-order chromaticity was corrected in 2007 [11] and that resulted in significant improvement of the proton lifetime.

At the end of Run II, the antiproton intensity lifetime deterioration due to the beam–beam effects was much smaller than the proton one, and was found to scale approximately as [7]

$$\left(\frac{1}{\tau_{\rm a}}\right)_{\rm BB} = \left(\frac{dN_{\rm a}}{N_{\rm a}dt}\right)_{\rm BB} \propto N_{\rm p}\frac{\varepsilon_{\rm a}^2}{S^3}, \tag{8.10}$$

where S stands for beam–beam separation (helix size).

Table 8.1 Tevatron luminosity and intensity loss rates averaged over the first 2 h of 2010–2011 HEP stores with initial luminosity from 300×10^{30} to 430×10^{30} $\mathrm{cm}^{-2}\ \mathrm{s}^{-1}$ in 2010–2011

	%/h	Incl. due to beam–beam, %/h
Proton loss rate, $1/\tau_{\mathrm{p}}$	2.8–3.2	1.5–2.0
Antiproton loss rate, $1/\tau_{\mathrm{a}}$	5.5–6.2	1.0–1.5
Emittance growth rate, $1/\tau_{\varepsilon}$	9–11	Small
H-factor decay rate, $1/\tau_{\mathrm{H}}$	1.2–1.4	Small
Luminosity decay rate, $1/\tau_{\mathrm{L}}$	19–21	2.5–3.5

8.2.3 Impact of Beam–Beam Effects on the Integrated Luminosity

The collider luminosity lifetime is determined by the speed of the emittance growth, beam intensity loss rates, and bunch lengthening (that affects hourglass factor H):

$$\tau_{\mathrm{L}}^{-1} = \frac{dL(t)}{L(t)dt} = \left|\tau_{\varepsilon}^{-1}\right| + \tau_{\mathrm{Na}}^{-1} + \tau_{\mathrm{Np}}^{-1} + \tau_{\mathrm{H}}^{-1}. \tag{8.11}$$

At the end of Run II, the luminosity loss rates were in the range 19–21 %/h at the beginning of stores—see Table 8.1. For the 2010–2011 HEP stores in range of initial luminosities between 3.0 and 4.3×10^{32} $\mathrm{cm}^{-2}\ \mathrm{s}^{-1}$, the largest contribution to luminosity decay came from beam emittance growth with a typical time of $\tau_{\varepsilon} \sim 9$–11 h. The growth is dominated by IBS in the proton bunches, with small contributions from the IBS in antiprotons and external noises. Beam–beam effects, if noticeable, usually manifest themselves in reduction of the beam emittances or their growth rates rather than in increases. The antiproton bunch intensity lifetime $\tau_{\mathrm{a}} \sim 16$–18 h is dominated by the luminosity burn rate which accounts for 80–85 % of the lifetime, while the remaining 10–15 % comes from parasitic beam–beam interactions with protons. Proton intensity loss varies in a wide range $\tau_{\mathrm{p}} \sim 25$–45 h and is driven mostly (~50 %) by the head-on beam–beam interactions with smaller size antiprotons at the main IPs. The proton lifetime caused by inelastic interactions with antiprotons in collisions and with residual gas molecules varies from 300 to 400 h. The hourglass factor decays with $\tau_{\mathrm{H}} \sim 70$–80 h due to the IBS, again, mostly in proton bunches. Beam–beam effects may lead to reduction of the proton bunch length growth (longitudinal "shaving") in a poorly tuned machine. Combining all of these loss rates together, one can estimate the hit on the luminosity lifetime τ_{L} due to the beam–beam effects as 12–17 % (that is equal to (2.5–3.5 %/h)/(19–21 %/h)). As concluded in [7], the luminosity integral $I = \int Ldt$—the sole critical parameter for HEP experiments—depends on the product of peak luminosity and the luminosity lifetime, e.g., for a single store with initial luminosity L_0 and duration $T \sim 16$ h, the integral is $I \approx L_0 \tau_{\mathrm{L}} \ln(1 + T/\tau_{\mathrm{L}})$. Therefore, the full impact of the beam–beam effects on the luminosity integral should include beam–beam-driven proton and antiproton losses at the injection energy (about 5 and 1 %,

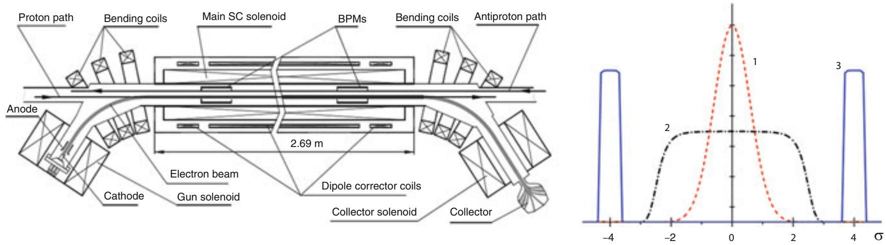

Fig. 8.12 General layout of the Tevatron electron lens; (*right*) transverse electron current profiles for (1) space-charge and head-on beam–beam compensation, (2) for bunch-by-bunch tune spread compensation, (3) halo collimation [19]

correspondingly), on the energy ramp (2 and 3 %), and in the low-beta squeeze (1–2 and 0.5 %) which proportionally reduce the initial luminosity L_0. So, altogether, at the last operational stage of the Tevatron collider present, the beam–beam effects reduce the luminosity integral by 23–33 %.

8.3 Tevatron Electron Lenses for Compensation of Beam–Beam Effects and Beam Collimation

Electron lenses employ electromagnetic fields of strongly magnetized high intensity electron beams and were originally proposed for compensation of the head-on beam–beam effects in the SSC [21] and for compensation of the long-range beam–beam effects in the Tevatron [22]. The lens employs a low energy beam of electrons which collides with the high-energy proton or antiproton bunches over an extended length. Electron space-charge forces are linear at distances smaller than the characteristic beam radius $r < a_e$ but scale as $1/r$ for $r > a_e$. Correspondingly, such a lens can be used for linear long-range beam–beam and nonlinear head-on beam–beam force compensation depending on the beam-size ratio a_e/σ and the current-density distribution $j_e(r)$. Electron lenses have also been proposed for compensation of space-charge forces in high intensity hadron accelerators [23]. Main advantages of the e-lenses are: (a) the electron beam acts on high-energy beams only through EM forces, with no nuclear interactions; (b) fresh electrons interact with the high-energy particles each turn, leaving no possibility for coherent instabilities; (c) the electron current profile (and, thus, the EM field profiles) can easily be changed for different applications—see Fig. 8.12; (d) the electron-beam current can be quickly varied, e.g., on a time scale of bunch spacing in accelerators.

Two electron lenses were built and installed in two different locations of the Tevatron p–pbar collider ring A11 and F48 [24]. They met specifications for the bunch-by-bunch tune spread compensation [17] and were used to counteract beam lifetime deterioration due to the long-range beam–beam effects [20] and for the abort gap beam removal [25] and for beam halo collimation [26]. Up to 3 A, 6–10 kV e-beam was generated at the 10–15 mm diameter thermocathode immersed in 0.3 T longitudinal magnetic field and aligned onto (anti)proton beam orbit over about 2 m length inside 6 T SC solenoid. The deviations of the magnetic field lines from a straight line are less than ±100 μm over the entire length of the SC solenoid. The electron beam, following the field lines, therefore does not deviate from the straight Tevatron beam trajectory by more than 20 % of the Tevatron beam rms size $\sigma \approx 0.5$–0.7 mm in the location of the TELs. In order to enable operation on a single bunch in the Tevatron with bunch spacing of 396 ns, the anode voltage, and consequently the beam current, is modulated with a characteristic on-off time of about 0.6 μs and a repetition rate equal to the Tevatron revolution frequency of $f_0 = 47.7$ kHz by using a HV Marx pulse generator [27] or a HV RF tube base amplifier. The electron pulse timing jitter is less than 1 ns and the peak current is stable to better than 1 %, so, the TEL operation does not incur any significant emittance growth.

The high-energy protons are focused by the TEL and experience a positive betatron tune shift:

$$dQ_{x,y} = +\frac{\beta_{x,y} L_e r_{\mathrm{p}}}{2\gamma ec} \cdot j_e \cdot \left(\frac{1-\beta_e}{\beta_e}\right). \tag{8.12}$$

In the long-range beam–beam compensation (BBC) experiments, large radius electron beam was generated $a_e \approx 3\sigma$; therefore, the tune shift was about the same for most protons in the bunch. The tuneshift for the antiprotons is of about the same magnitude, but negative. Maximum measured tuneshift for 980 GeV protons was about 0.01.

In the BBC demonstration experiment [20], the electron beam of the TEL-2 installed at the A11 location with large vertical beta-function of $\beta_y = 150$ m was centered and timed onto bunch #12 without affecting any other bunches. When the TEL peak current was increased to $J_e = 0.6$ A, the lifetime $\tau = N/(dN/dt)$ of bunch #12 went up to 26.6 h from about 12 h—see Fig. 8.13. At the same time, the lifetime of bunch #36, an equivalent bunch in the third bunch train, remained low and did not change significantly (at 13.4 h lifetime). When the TEL current was turned off for 15 min, the lifetimes of both bunches were, as expected, nearly identical (16 h). The TEL was then turned on again, and once again the lifetime for bunch #12 improved significantly to 43 h while bunch #36 stayed poor at 23.5 h. This experiment demonstrates a factor of two improvement in the proton lifetime due to compensation of beam–beam effects with the TEL.

The proton lifetime, dominated by beam–beam effects, gradually improves and reaches roughly 100 h after 6–8 h of collisions; this is explained by a decrease in antiproton population and an increase in antiproton emittance, both contributing to a reduction of the proton beam–beam parameter. To study the effectiveness of BBC later in the store, the TEL was repeatedly turned on and off every half hour for 16 h, again on bunch #12. The relative improvement R, defined as the ratio of the proton

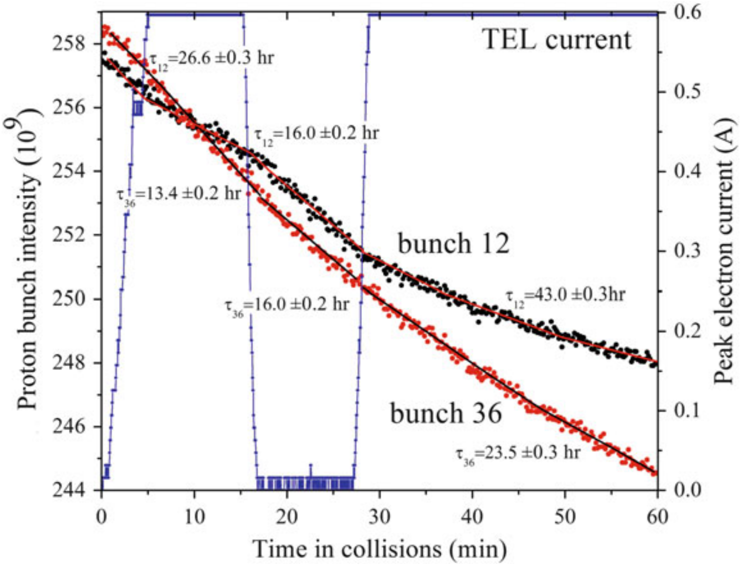

Fig. 8.13 Intensities of proton bunches #12 and #36 early in store #5119 with $L_0 = 1.6 \times 10^{32}$ cm^{-2} s^{-1} [20]

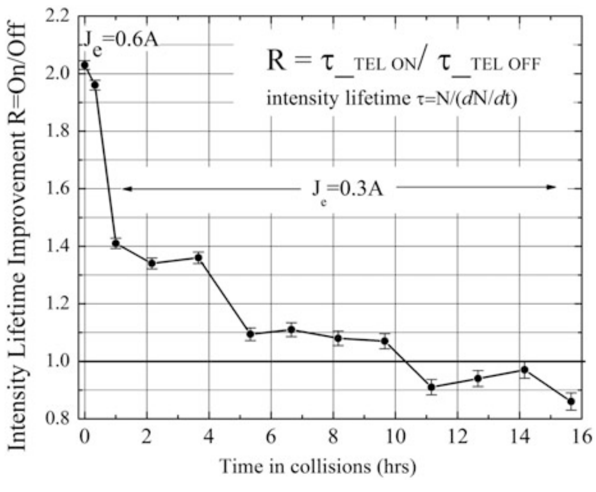

Fig. 8.14 Relative improvement of proton bunch #12 lifetime induced by TEL vs. time in store #5119 [20]

lifetime with the TEL and without, is plotted in Fig. 8.14. The first two data points correspond to $J_e = 0.6$ A (as is Fig. 8.13 and the above description), but subsequent points were taken with $J_e = 0.3$ A to observe dependence of the compensation effect on electron current. The change of the current resulted in a drop of the relative improvement from $R = 2.03$ to $R = 1.4$. A gradual decrease in the relative improvement is visible until after about 10 h, where the ratio reaches 1.0 (no gain in lifetime). At this point, the beam–beam effects have become very small, providing little to compensate. Similar experiments in several other stores with initial luminosities ranging from L_0=1.5×10^{32} cm^{-2} s^{-1} to 2.5×10^{32} cm^{-2} s^{-1} repeated these results.

The lifetime improvement due to the TEL can be explained in part by the positive shift of vertical tune of protons $dQ_y \approx 0.0015$ which makes the detrimental effects of the twelfth-order resonance $Q_y = 7/12 = 0.583$ weaker. The average Tevatron proton tune $Q_y = 0.589$ (which is carefully optimized to minimize overall losses) is just above this resonance, and the bunches at the end of each train, which have vertical tunes lower by $\Delta Q_y = -(0.002$–$0.003)$ due to unique pattern of long-range interactions, are subject to stronger beam–beam effects (see preceding section). The TEL moves those protons away from the resonance, thus, resulting in significant reduction of the losses. It is noteworthy, that the TEL operation with $J_e = 0.6$ A resulted in bunch #12 having one of the lowest loss rates among all bunches, while its tune still remained lower $dQ_y < |\Delta Q_y|$.

Results of many experiments with TEL are reported in [19], studies of nonlinear BBC with Gaussian electron-beam current profile are presented in [28]. TELs were not used routinely for the BBC in the Tevatron because beam–beam losses were effectively controlled by other means as described in Sect. 8.2. Numerical simulations [29] predict beneficial effect of electron lenses on the ultimate intensity LHC beam lifetime.

8.4 Modeling and Simulation of Beam–Beam Effects in Tevatron

In this section we describe the models and simulation tools, which were used to study beam–beam effects in the Tevatron. Simulations correctly describe many observed features of the beam dynamics, have predictive power, and have been particularly useful for supporting and planning changes of the machine configuration. For the sake of brevity we mostly concentrate on effects occurring during high-energy physics operation.

8.4.1 Store Beam Physics Analysis

Beam–beam interaction is not the single strongest effect determining evolution of beam parameters at collisions. There are many sources of diffusion causing emittance growth and particle losses, including but not limited to intrabeam scattering, noise of accelerating RF voltage, and scattering on residual gas. Parameters of these mechanisms were measured in beam studies, and then a model was built in which

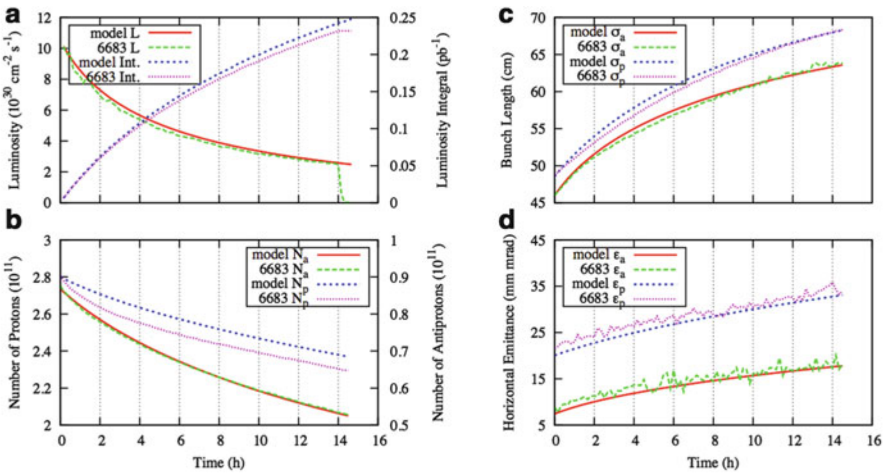

Fig. 8.15 Observed beam parameters in store 6683 compared to store analysis calculation (model). $L_0 = 3.5 \times 10^{32}$ cm^{-2} s^{-1}. (**a**) Single bunch Luminosity and Luminosity integral. (**b**) Intensity of proton bunch no. 6 and of antiproton bunch colliding with it (no. 13). (**c**) Bunch lengths. (**d**) Horizontal 95 % normalized bunch emittances [8]

the equations of diffusion and other processes are solved numerically. The model, which is described in detail in Sect. 6.4, is able to predict evolution of the beam parameters in the case of weak beam–beam effects. When these effects are not small, it provides a reference for evaluation of their strength. This approach was used on a store-by-store basis to monitor the machine performance in real time because such calculations are very fast compared to a full numerical beam–beam simulation. Figure 8.15 presents an example comparison of evolution of beam parameters in an actual high-luminosity store to calculations. Note that there is no transverse emittance blow up in both beams, and processes other than beam–beam interaction determine the emittance growth. The same is true for antiproton intensity and bunch length. The most pronounced difference between the observation and the model is seen in the proton intensity. Beam–beam effects cause proton lifetime degradation during the initial 2–3 h of the store until the proton beam–beam tune shift drops from 0.02 to 0.015. The corresponding loss of luminosity integral is about 5 %.

8.4.2 *Weak-Strong Numerical Simulations*

Simulations, in which the "strong" beam is considered as having constant and known distribution and is usually represented by a formula, while the other, "weak," beam is modeled as a bunch of macro-particles, are a convenient tool for predicting evolution of beam intensity and emittance caused by incoherent effects. Since such simulation does not necessitate multi-bunch treatment of beam dynamics, the tracking of 10^4 macro-particles through the Tevatron lattice with two head-on and 70 long-range collision points for 10^7 turns (which correspond to approximately 3 min of real time) takes about 20 h. One of the codes that found wide use for simulation of the Tevatron beam–beam phenomena is Lifetrac [30]. Originally, Lifetrac was developed for simulation of equilibrium distribution of particles in circular electron-positron colliders. In 1999 new features have been implemented, which allowed simulating non-equilibrium distributions, for example proton beams. In this case the goal of simulations is not to obtain the equilibrium distribution but to observe how the initial distribution is changing with time. Number of simulated particles typically varies in the range of 10^3–10^6. The tracking time is divided into "steps," typically 10^3–10^5 turns each. The statistics obtained during the tracking (1D histograms, 2D density in the space of normalized betatron amplitudes, luminosity, beam sizes, and emittances) is averaged over all particles and all turns for each step. Thus, a sequence of frames representing evolution of the initial distribution is obtained.

Another important quantity characterizing the beam dynamics is the intensity lifetime. It is calculated by placing an aperture restriction in the machine and counting particles reaching the limit. The initial and final coordinates of the lost particle are saved. This information is valuable for analysis of various beam dynamics features.

The initial 6D distribution of macro-particles can be either Gaussian (by default), or read from a separate text file. Besides, the macro-particles may have different "weights." This allows representing the beam tails more reliably with limited number of particles. Usually we simulate the Gaussian distribution with weights: particles initially located in the core region have larger weight while the "tail" particles with smaller weight are more numerous.

When performing tracking through a head-on IP, the "strong" bunch is divided into slices longitudinally. The higher are the orders of significant betatron resonances, which make effect on the distribution, the greater must be the number of slices. In our simulations 12 slices were used in the main IPs where beta-functions are approximately equal to the bunch length and only one slice in long-range collision points where beta-functions are much greater and one can neglect the betatron phase advance on the bunch length.

The transverse density distributions within "strong" slices are bi-Gaussian, allowing to apply the well-known formulae [31] for 6D symplectic beam−beam kick. However, a simple modification allowed simulating non-Gaussian strong bunches. Namely, the strong bunch is represented as a superposition of a few (up to three) Gaussian distributions with different betatron emittances. The kicks from all these "harmonics" are added. The calculation time is increased but the transformation remains 6D symplectic.

To study the dependence of beam−beam effects on various machine parameters, the following features were incorporated into the code:

- Realistic machine optics via linear 6D maps calculated from actual beam measurement data (Sect. 4.2), with full account of betatron coupling and optics differences on the proton and antiproton orbits. It was estimated that resonances generated by known Tevatron nonlinearities, such as the final focus triplets and lattice sextupoles, are much weaker than those driven by beam−beam collisions at the present betatron tune working point. Hence, inclusion of nonlinear lattice elements into the simulation was deemed unnecessary. Still, the code has the capability to include thin multipoles up to the tenth order.
- Collision point pattern individual for each bunch within the train, with beams separations obtained from beam measurements.
- First- and second-order chromaticity implemented as symplectic "chromatic drifts." In the Hamiltonian theory the chromaticity of beta-functions does not come from energy-dependent focusing strength of quads (as one would intuitively expect) but from drift spaces where the transverse momentum is large (low-beta regions). The symplectic transformations for that are

$$\begin{array}{l} x = x - L \cdot x' \cdot \delta \\ y = y - L \cdot y' \cdot \delta \\ z = z - L(x'^2 + y'^2)/2 \end{array},$$

where x, y, and z are the particle coordinates, $\delta = \Delta p/p$ is the momentum deviation, and L is the "chromatic drift" length. Then, it is necessary to adjust the betatron tune chromaticities, which are also affected by "chromatic drift." For that, an artificial element (insertion) is used with the following Hamiltonian:

$$H = I_x(2\pi Q_x + C_x\delta) + I_y\left(2\pi Q_y + C_y\delta\right), \tag{8.13}$$

where I_x and I_y are the action variables, Q_x and Q_y are the betatron tunes, C_x and C_y are the [additions to the] chromaticities of betatron tunes.

- Diffusion and noise, in the form of a random Gaussian kick applied to macroparticles once per turn. Strength of the kick on different coordinates is given by a symmetrical matrix representing correlations between Gaussian noises. In the Tevatron, the diffusion is rather slow in terms of the computer simulation—the characteristic time for the emittance change is around an hour or 10^8 turns. In simulations aimed at evaluation of the antiproton beam dynamics during the 2004–2005 run the noise was artificially increased by three orders of magnitude in order to match the diffusion and the computer capabilities [4].
- Beam–beam compensator (electron lens) element implemented as a thin nonlinear lens.

We have validated the code using available experimental data. As an example, Figs. 8.16 and 8.17 show a good reproduction of the two distinct effects in bunch-to-bunch differences caused by beam–beam effects: variation of vertical bunch centroid position due to long-range dipole kicks, and variation of transverse emittance blowup caused by difference in tunes and chromaticities.

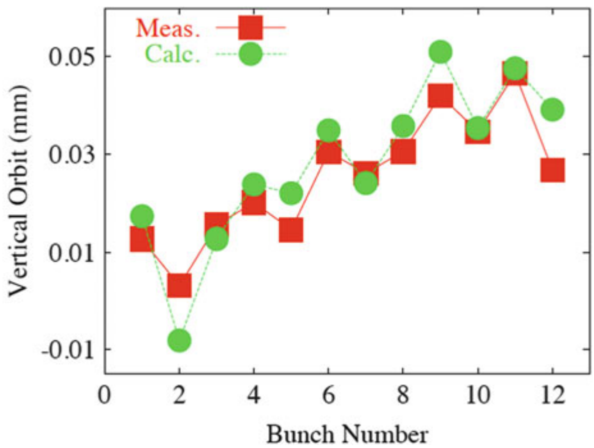

Fig. 8.16 Bunch-by-bunch antiproton vertical orbit [8]

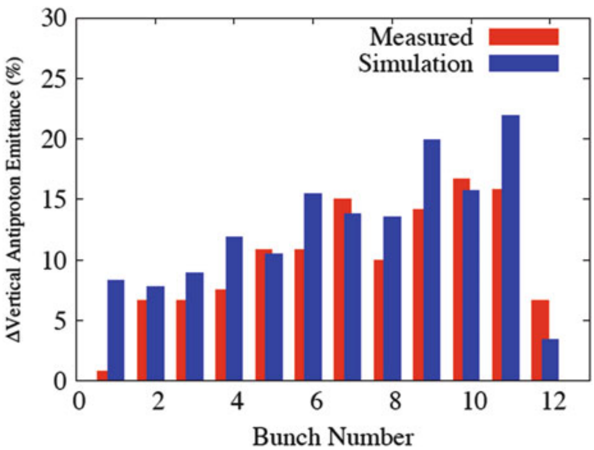

Fig. 8.17 Bunch-by-bunch antiproton emittance growth. Measured in store #3554 (*red*) and simulated with lifetrac (*blue*) [8]

Lifetrac simulations proved to be a useful tool in justification and development of machine upgrades, such as

- The decrease of antiproton betatron tune chromaticity, reduction of the β^* from 0.35 to 0.28 m (both in 2005).
- Demonstration of the importance of separation at long-range collision points nearest to the main IPs, and subsequent implementation of the new collision helix.
- Identification of the large chromaticity of β^* as a possible source of lifetime deterioration following the increase of the antiproton intensity. Simulations revealed an interesting feature in the behavior of the proton bunch length at high values of beam–beam parameter ξ—the so-called bunch shaving, when the bunch length starts to decrease after initiating head-on collisions instead of steady growth predicted by the diffusion model (Fig. 8.18). This behavior was

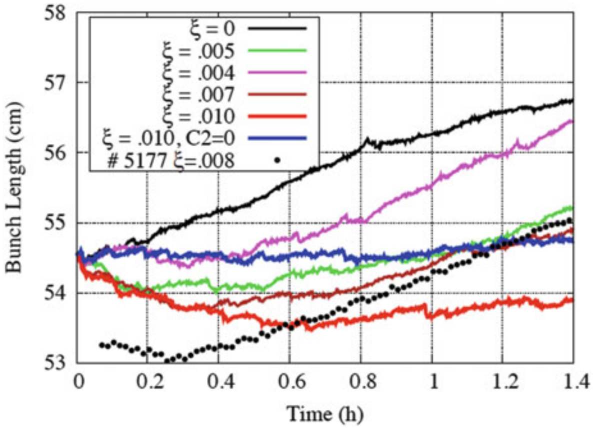

Fig. 8.18 Effect of corrected second-order chromaticity on the proton bunch length evolution. *Solid lines*—simulation for different ξ, *black dots*—experimental data [8]

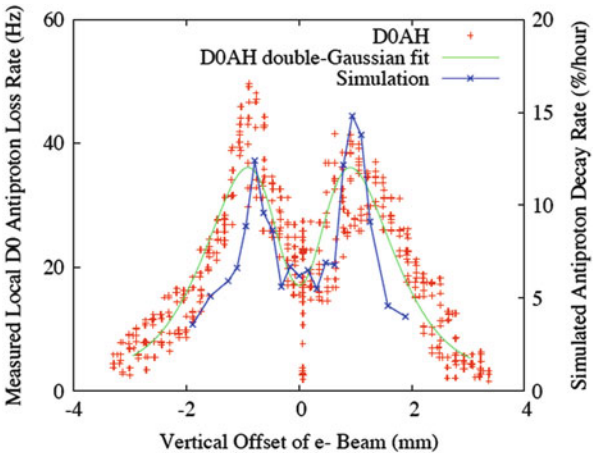

Fig. 8.19 Measured (*red crosses*, D0AH), and simulated particle loss rate during a vertical TEL-beam separation scan

observed multiple times during HEP stores in 2007, being especially pronounced when the vertical proton betatron tune was set too high.

- With the use of Lifetrac, it was shown that a change of the tune working point from 0.58 to near the half integer resonance would allow as much as 30 % increase of intensities but such upgrade required a lengthy commissioning period and was not realized during Run II.
- Lifetrac was routinely used to support beam physics studies, e.g., the experiments on BBC with electron lenses (see preceding section 8.3). For instance, Fig. 8.19 presents the measured and simulated particle loss rate during a transverse separation scan between the circulating beam and the Gaussian TEL beam.

8.4.3 Strong–Strong Numerical Simulations

Although coherent beam–beam effects did not present a limitation of the machine performance, extensive work has been done to create an accurate model of multi-bunch collective dynamics [32]. A comprehensive Tevatron simulation was created including a fully 3D strong–strong beam–beam particle-in-cell Poisson solver, interactions among multiple bunches with both head-on and long-range collisions, a linear optics model using measured coupled lattice functions, a helical trajectory consistent with beam-orbit measurements, and machine chromaticity and impedance.

The starting point for the simulation is the extended BeamBeam3d code [33, 34]. Bunches of macro-particles in two beams are generated with a random distribution in phase space with parameters that match the lattice. The accelerator ring is conceptually divided into arcs with potential interaction points at the ends of the arcs. All bunches from both beams are individually tracked. When bunches from two beams arrive at the same IP, a Poisson field solver is employed to determine the electromagnetic forces on each particle produced by the charged particles in the opposing beam bunch. Beam–beam forces in extended length bunches are computed by slicing the bunch longitudinally and moving the bunches through other in steps, applying the beam–beam forces at each step. The optics of each arc is modeled with a 6×6 linear map that transforms the phase space $\{x, x', y, y', z, \delta\}$ coordinates of each macro-particle from one end of the arc to the other. For our Tevatron simulations, the maps were calculated using the measured coupled lattice functions (see Chap. 2). The synchrotron motion is put in as a sinusoidal oscillation with the periodicity of the machine synchrotron tune. A shifted Greens function is employed in the Poisson field solver calculation to efficiently account for the mean beam transverse offset at each IP. The validity of the 3D beam–beam calculation has been verified [34] by reproducing the evolution [35] of synchrobetatron modes observed at the VEPP-2M e+$e-$ collider as a function of beam–beam parameter ξ.

The impedance model applies a momentum kick to the particles generated by the dipole component of resistive wall wakefields [36]. Each beam bunch is divided longitudinally into slices containing approximately equal numbers of particles. As each bunch is transported through an arc, particles in each slice receive a transverse kick from the wakefield induced by the dipole moment of the particles in forward slices. The impedance model has been verified to agree with analytic calculations of instability thresholds and growth rates for the two macro-particle model of strong and weak head-tail instabilities [34, 36].

During the Tevatron operation in 2009 the limit for increasing the initial luminosity was determined by particle losses in the squeeze [37]. With proton bunch intensities approaching 3.2×10^{11} particles, the chromaticity of the Tevatron had to be managed carefully to avoid the development of a head-tail instability. It was determined experimentally that, after the head-on collisions are initiated, the Landau damping introduced by beam–beam interaction is strong enough to maintain beam stability at chromaticity of +2 units. At the earlier stages of the collider cycle, when beam–beam effects are limited to long-range interactions, the chromaticity was kept as high as 15 units since the concern was that the Landau damping is insufficient to suppress the instability. At the same time, high chromaticity causes particle losses, which are often large enough to quench the superconducting magnets, and hence it is desirable to keep it at a reasonable minimum.

The strong–strong simulation was used to determine the safe lower limit for chromaticity. Simulations demonstrated that for the Tevatron parameters, long-range beam–beam interactions provide stabilization of the head-tail instability. Based on these findings, the chromaticity in the squeeze was lowered by a factor of 2, and was kept at 8–9 units. This resulted in a significant decrease of the observed particle loss rates (see, e.g., Fig. 5 in [37]).

References

1. T. Sen, arXiv:1102.2432 (2010); also in ICFA Beam Dyn. Newslett. **52**, 14–32 (2010)
2. R. Moore, A. Jansson, V. Shiltsev, JINST **4**, P12018 (2009)
3. T. Sen et al., Rev. ST Accel. Beams **7**, 041001 (2004)
4. Y. Alexahin, in *Proceedings of 2005 IEEE Particle Accelerator Conference,* Knoxville (2005), p. 544
5. S. Saritepe, G. Goderre, S. Peggs, in *Frontiers of Particle Beams: Intensity Limitations*, Springer, Lecture Notes in Physics (1991)
6. V. Bharadwaj, et al., *FNAL Preprint Fermilab-TM-1970* (1996)
7. V. Shiltsev et al., Phys. Rev. ST Accel. Beams **8**, 101001 (2005)
8. A. Valishev, et al., JINST **7**, P12002 (2012); also arXiv:0906.0386 (2009)
9. P. Ivanov, et al., in *Proceedings of the 2003 IEEE Particle Accelerator Conference*, Portland, OR (2003), p. 3062
10. Y. Alexahin, in *Proceedings of the 2007 IEEE Particle Accelerator Conference*, Albuquerque, NM (2007), pp. 3874–3876
11. A. Valishev, G. Annala, V. Lebedev, R. Moore, in *Proceedings of the Particle Accelerator Conference*, Albuquerque, NM (2007), p. 3922
12. M. Syphers, *Beam-Beam Tune Distributions with Differing Beam Sizes,* Fermilab internal document Beams-Doc-3031 (2008)
13. C.Y. Tan, J. Steimel, in *Proceedings of the 2009 IEEE Particle Accelerator Conference*, Vancouver, Canada (2009), p. 1668
14. P. Bagley, et al., *FNAL Preprint Conf-96-392* (1996)
15. L. Michelotti, *FNAL Preprint TM-1738* (1995)
16. R. Pasquinelli, A. Jansson, Phys. Rev. ST Accel. Beams **14**, 072803 (2011)
17. Y. Alexahin, *Preprint FERMILAB-PUB-00-120-T* (2000)
18. T. Sen et al., Phys. Rev. ST Accel. Beams **7**, 0410101 (2004)
19. V. Shitsev et al., New J. Phys. **10**, 043042 (2008)
20. V. Shiltsev et al., Phys. Rev. Lett. **99**, 244801 (2007)
21. E. Tsyganov, A. Taratin, A. Zinchenko, Phys. Part. Nuclei **27**, 279 (1996)
22. V. Shiltsev et al., Phys. Rev. ST Accel. Beams **2**, 071001 (1999)
23. A. Burov, G. Foster, V. Shiltsev, *Fermilab Preprint FNAL-TM-2125* (2000)
24. V. Shiltsev et al., Phys. Rev. ST Accel. Beams **11**, 103501 (2008)
25. X.-L. Zhang et al., Phys. Rev. ST Accel. Beams **11**, 051002 (2008)
26. V. Shiltsev, in *Proceedings of BEAM'06* (Valencia, Spain), Yellow Report CERN-2007-002; G. Stancari, et al., Phys. Rev. Lett. **107**, 084802 (2011)

27. H. Pfeffer, G. Saewert, JINST **6**, P11003 (2011)
28. A. Valishev, et al., in *Proceedings of 2010 International Particle Accelerator Conference*, Kyoto, Japan (2010), p. 2084
29. A. Valishev, V. Shiltsev, in *Proceedings of the 2009 IEEE Particle Accelerator Conference*, Vancouver, Canada (2009), p. 2567
30. D. Shatilov, Part. Accel. **52**, 65 (1996)
31. K. Hirata, H. Moshammer, F. Ruggiero, *KEK Report 92-117* (1992)
32. E. Stern, J.F. Amundson, P.G. Spentzouris, A.A. Valishev, Fully 3D multiple beam dynamics processes simulation for the Tevatron. Phys. Rev. ST Accel. Beams **13**, 021003 (2010)
33. J. Qiang, M.A. Furman, R.D. Ryne, J. Comp. Phys. **198**, 278–294 (2004)
34. E. Stern, et al., in *Proceedings of IEEE PAC07*, Albuquerque, NM (2007), p. 905
35. I.N. Nesterenko, E.A. Perevedentsev, A.A. Valishev, Phys. Rev. E, **65**, 056502 (2002)
36. A. Chao, *Physics of Collective Beam Instabilities in High Energy Accelerators* (Wiley, New York, 1993), pp. 56–60, 178–187, 333–360
37. A. Valishev, et al., *in Proceedings of the 2009 IEEE Particle Accelerator Conference*, Vancouver, Canada (2009), p. 4230